JOURNAL OF GEOPHYSICAL RESEARCH, VOL. 115, D03102, doi:10.1029/2009JD012811, 2010

Impact of mesoscale vegetation heterogeneities on the dynamical and thermodynamic properties of the planetary boundary layer

Luis Garcia-Carreras,[1] Douglas J. Parker,[1] Christopher M. Taylor,[2] Claire E. Reeves,[3] and Jennifer G. Murphy[4]

Received 9 July 2009; revised 24 September 2009; accepted 2 October 2009; published 3 February 2010.

[1] This study uses aircraft observations over the Republic of Benin from the African Monsoon Multidisciplinary Analyses (AMMA) campaign to investigate the impact of vegetation heterogeneities on the dynamics within the planetary boundary layer, such as convection, transport, and mixing. Isoprene, a biogenic volatile organic compound emitted primarily by woody vegetation, was used as a tracer for transport to link the land surface to the boundary layer properties. Associated to planetary boundary layer (PBL) temperature gradients at vegetation boundaries, a persistent mesoscale organization of the winds which controlled patterns in the formation of cumulus congestus clouds was observed. A strong relationship among PBL temperatures, meridional wind velocity, isoprene concentrations, and fraction of forest or shrub cover was found, corroborating the land surface forcing of the observed dynamics. The observations show that the convergence zones tended to occur on the southern edge of warm surface and atmospheric anomalies. The northerly synoptic wind appears to have increased the coherency of the southerly part of the mesoscale flow and displaced the convergence zones southward. The relationships between the PBL potential temperatures and the meridional wind and isoprene concentrations were spatially coherent down to wavelengths of 10 and 8 km, respectively. A seasonal climatology of visible satellite data shows enhanced cloud cover in the afternoon over cropland, suggesting that the results presented are not limited to this case study but are of climatological significance in the region.

Citation: Garcia-Carreras, L., D. J. Parker, C. M. Taylor, C. E. Reeves, and J. G. Murphy (2010), Impact of mesoscale vegetation heterogeneities on the dynamical and thermodynamic properties of the planetary boundary layer, *J. Geophys. Res.*, *115*, D03102, doi:10.1029/2009JD012811.

1. Introduction

[2] Variations in the land surface vegetation cover can affect the surface energy and moisture budgets, which in turn alter the planetary boundary layer (PBL). The PBL is defined here as "the part of the troposphere that is directly influenced by the presence of the Earth's surface" [*Stull*, 1988, p. 2]. Vegetation affects properties such as albedo, roughness length, and leaf area index, which control surface fluxes of heat and water. Variations in these fluxes can then potentially impact the dynamics and growth of the PBL, the development of convective clouds via changes in, for example, the convective available potential energy (CAPE) [*Segal et al.*, 1995], and therefore the surface radiative fluxes and amount and distribution of precipitation [*Pielke*, 2001]. These changes can then potentially feed back into the land surface via changes in soil moisture and vegetation patterns.

[3] At the mesoscale, heterogeneities in surface characteristics, and thus surface fluxes, can lead to sharp gradients in PBL temperatures which may force local circulations analogous to "sea breezes" (see *Segal and Arritt* [1992] for a comprehensive review). There are many modeling studies that confirm the presence of these circulations for boundaries between different vegetation types [*Hong et al.*, 1995; *Pinty et al.*, 1989]. These, as well as theoretical studies such as *Baldi et al.* [2008], show that the necessary length scale of the heterogeneities for these circulations to develop must be approximately 10–100 km, although at low latitudes the impact is maximized for the lowest length scales within this range [*Wang et al.*, 1996]. For smaller length scales, turbulent eddies during the day will tend to destroy these temperature gradients before a circulation can develop (e.g., as shown in the work of *Linden and Simpson* [1986] in laboratory experiments).

[4] Synoptic conditions can also play a significant role on the nature of the circulations. Although some studies suggest that synoptic conditions must be weak for these circulations to develop [*Avissar and Schmidt*, 1998], there is some evidence to the contrary. Mesoscale modeling by

[1]Institute for Climate and Atmospheric Science, University of Leeds, Leeds, UK.
[2]Centre for Ecology and Hydrology, Wallingford, UK.
[3]School of Environmental Science, University of East Anglia, Norwich, UK.
[4]Department of Chemistry, University of Toronto, Toronto, Canada.

0148-0227/10/2009JD012811$09.00

Weaver [2004] shows that the background flow can affect the shape and orientation of the mesoscale circulations but has a lesser impact on their intensity. The orientation of the synoptic flow can also significantly affect the depth and intensity of the mesoscale circulations, which usually reach a height of 10–30% of the PBL height [*Simpson and Britter*, 1980]. High-resolution modeling of opposing sea breezes over Cape York Peninsula in Australia [*Goler and Reeder*, 2004] as well as laboratory experiments on gravity currents [*Simpson and Britter*, 1980] show that the presence of a head wind leads to a shallower and more coherent circulation, given by stronger potential temperature anomalies and sharper gradients between the airflows in the mixed layer. A tail wind, on the other hand, will act to deepen the circulation and reduce the thermal and wind gradients (see also discussion by *Parker* [1998]).

[5] The convergence lines associated with land surface–induced mesoscale circulations can impact convective initiation. *Wilson and Schreiber* [1986] carry out a statistical analysis of convective storms near the Colorado Rocky Mountains and find that 95% of the most intense storms were initiated by mesoscale boundary layer convergence lines, although the origin of the convergence was unknown. Mesoscale flows can moisten the atmosphere above the area with the greatest sensible heating, thus increasing CAPE and lowering the convective inhibition. The circulations can then directly trigger deep convection [*Trier et al.*, 2004]. *Taylor et al.* [2009] document a case of a major convective storm triggering on a soil moisture gradient in the Sahel. Despite the fact that land surface–induced mesoscale circulations will generally be unresolved by general circulation models, these studies suggest that their impact can be significant for the correct prediction of convective initiation and, thus, precipitation.

[6] Despite the considerable number of modeling studies corroborating the presence and significance of land surface–induced mesoscale circulations, there are few observational studies demonstrating their existence because of real life heterogeneities not being as well defined as in the modeling studies as well as the difficulty of decoupling any local, land-induced effects from the synoptic flow. Some studies, however, have measured a significant mean across-boundary wind anomaly between native vegetation and cropland [*Doran et al.*, 1995; *Smith et al.*, 1994; *Souza et al.*, 2000] which is attributed to land surface impacts. Other studies have found that the mean low-level cloud cover from satellite imagery is, in certain regions, closely related to deforestation patterns [*Cutrim et al.*, 1995; *Wang et al.*, 2009] or the presence of cropland [*Brown and Arnold*, 1998; *Rabin et al.*, 1990]. In all these studies, the observations are attributed to PBL temperature differences caused by variations in the sensible heat flux over the different vegetation types. *Taylor et al.* [2003] observe a coherent thermodynamic response to the surface, following which *Taylor et al.* [2007] and *Kang et al.* [2007] use aircraft data to provide direct observations of a land surface–induced circulation in the Sahel and USA, respectively, although in both cases these were forced by soil moisture patterns.

[7] The mesoscale can be of considerable significance for the transport and mixing of chemical species, although this is poorly resolved in global models. *Devine et al.* [2006] find that transport of dimethyl sulphide (DMS) into the troposphere, a chemical species with a wind-dependent source strength from the ocean [*Liss and Merlivat*, 1986], was underestimated by 50% because of secondary convection occurring at the edges of cold pools, where DMS concentrations were also higher than the domain average. Tethered balloon measurements made in the PBL over a rural and an urban site in the USA show that isoprene concentrations at 200–300 m are strongly influenced by the mixed layer depth [*Andronache et al.*, 1994]. The mixed layer depth, on the other hand, can be closely related to variations in the land surface when sensible heat flux contrasts are strong. Radiosonde data from Rondônia in the Amazon show boundary layer depth differences of 550 m between pasture and forest [*Fisch et al.*, 2004]. Given the aforementioned impact of vegetation and soil moisture heterogeneities on mesoscale flows, transport in the mesoscale could lead to significant deviations from global model estimates.

[8] In this study, isoprene is used as a tracer to link land surface features to the PBL characteristics. Isoprene (C_5H_8) is a biogenic volatile organic compound which is emitted in varying degrees by vegetation, although it is more closely related to woody species as opposed to herbs and crops [*Kesselmeier and Staudt*, 1999]. On average, forest or shrubland tropical ecosystems have base emission rates 3 times as high as cropland [*Guenther et al.*, 1995]. The main environmental controls which govern emissions are temperature and photosynthetically active radiation [*Kesselmeier and Staudt*, 1999]. Therefore, when these environmental factors are spatially similar, changes in vegetation cover type and density will be expected to control variations in isoprene emissions. During daylight the lifetime of isoprene is less than 1 h [*Atkinson*, 1986] (when assuming OH concentrations above 3×10^6 molecules cm^{-3}), and as a result of this short lifetime, the spatial pattern in abundance closely matches the spatial patterns in vegetative emissions.

[9] This study presents direct observations of land surface–induced circulations forced by vegetation heterogeneities using aircraft data from the African Monsoon Multidisciplinary Analyses (AMMA) campaign: the work presents a complementary study to that of [*Taylor et al.*, 2007] for the soil moisture case. The objectives of this paper are to assess the impact of vegetation heterogeneities on the dynamics in the PBL and their impact on convection, transport, and mixing. Section 2 gives an overview of the data sets used and the synoptic conditions present on 17 August 2006. Section 3 presents aircraft observations of the mesoscale circulation and its relationship with the land surface. The observed relationships and their length scale dependence are then quantified using cospectral analysis in section 4. In section 5 satellite data are used to explore the diurnal evolution of the mean cloud cover along the flight path throughout the monsoon season. Finally, section 6 discusses the results and presents conclusions.

2. Data and Conditions on 17 August 2006

[10] This case study uses data from a flight on 17 August 2006 of the Facility for Airborne Atmospheric Measurements (available at http://www.faam.ac.uk/) UK BAe-146 atmospheric research aircraft as part of the monsoon special observing period of the AMMA observational campaign

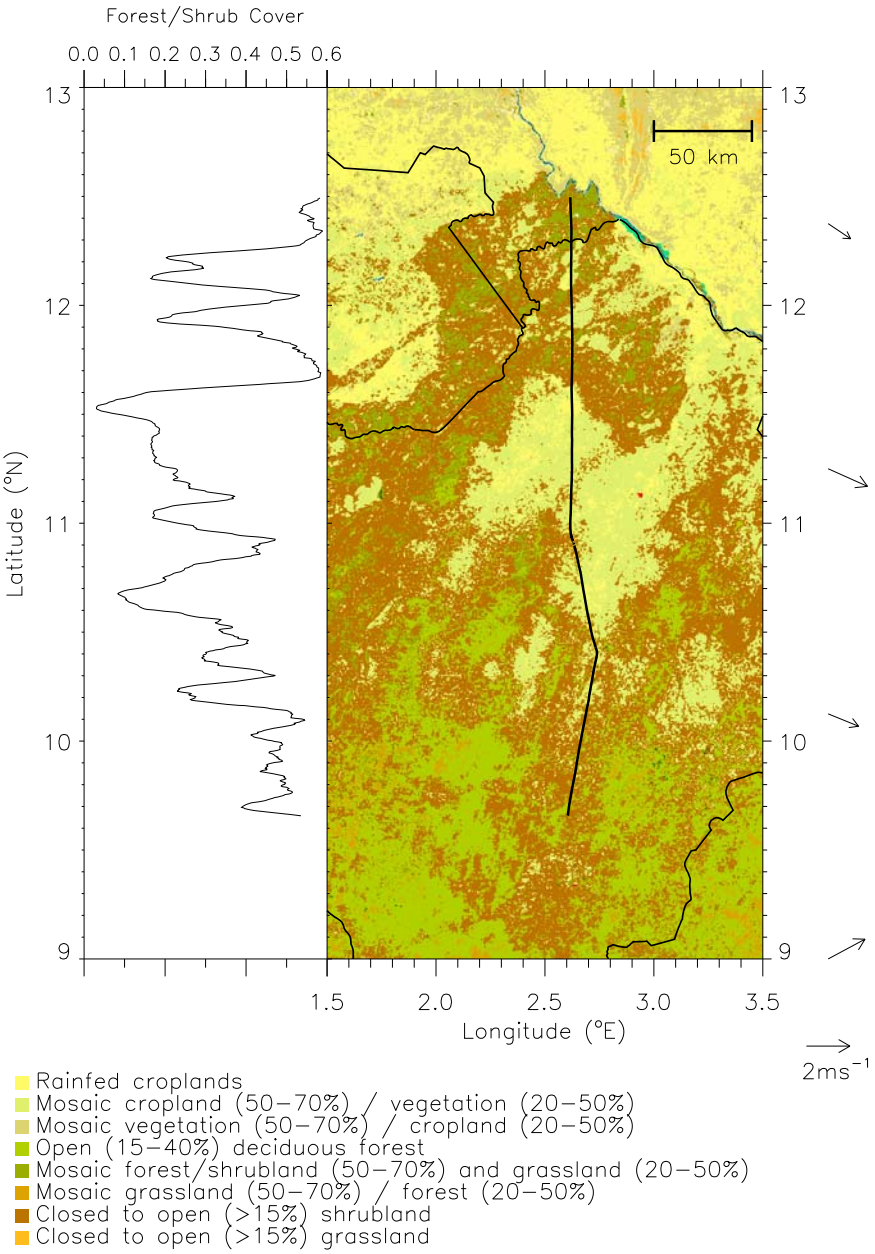

Figure 1. (left) Fraction of forest or shrub cover as estimated for each point along the flight path from the GlobCover classification system and averaged over a length scale of 5 km, and (right) the GlobCover Land Cover map with the low-level flight path (solid line). The map is derived from a time series of MERIS FR mosaics using the UN Land Cover Classification System (source data is copyright ESA and ESA GlobCover Project, led by MEDIAS-France/POSTEL). The vectors on the right show the wind speed and direction derived from the 1.125° resolution EMCWF 1200 UTC operational analysis at 925 hPa.

[*Lebel et al.*, 2009; *Redelsperger et al.*, 2006]. The flight was targeting the contrast between mesoscale forest features associated with Parc W, an area of protected natural vegetation, and the extensive fields surrounding it. The flight covered a north-south track of 325 km from Niger into the Republic of Benin and took place in the early afternoon, when the atmospheric response to the land surface would be maximized, but the rate of change of PBL properties was relatively slow. The topography along the flight path was relatively flat, varying from 200 to 400 m above sea level, with maximum variations of 50 m in the region between 10.7°N and 12°N, which is the focus of the majority of this analysis. The closest topographic peak above 1000 m lies approximately 600 km east of the flight track. This case study uses data from two legs; a southward leg through a cumulus congestus cloud layer at a mean altitude of 1150 m above ground level (1253–1340 UTC) and the return leg at a lower mean altitude of 190 m above ground level (1346–1431 UTC). Data used include temperature and three-dimensional wind observations at 1 Hz, liquid water content

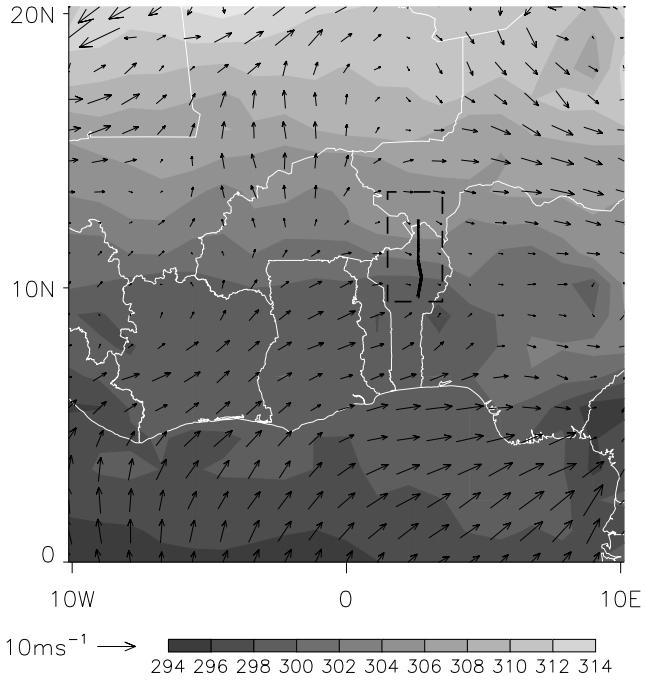

Figure 2. Temperature at the lowest model level (shading) and 925 hPa wind vectors from the 1.125° resolution EMCWF 1200 UTC operational analysis. The solid black line shows the low-level flight path and the dashed rectangle shows the domain for Figure 1.

from the Johnson-Williams instrument at 4 Hz [*Strapp and Schemenauer*, 1982], and isoprene concentrations measured using a proton transfer reaction mass spectrometer (PTR-MS) (manufactured by Ionicon Analytik and adapted for aircraft use) with a dwell time of 1 s in each 15 s sample cycle.

[11] Land surface features are identified using the GlobCover Land Cover satellite remote sensing product. This is an automatic and regionally tuned classification of a time series of Medium-Resolution Imaging Spectrometer (MERIS) Full Resolution (FR) mosaics using the UN Land Cover Classification System (source data is copyright ESA and ESA GlobCover Project, led by Mediterranée et Afrique Subtropicale (MEDIAS)–France and Pôle d'Observation des Surfaces Terrestres aux Echelles Larges (POSTEL)). The GlobCover Land Cover map is here used primarily to differentiate between regions of forest/shrubland and cropland. Figure 1 (right) shows the different land surface types in the region around the flight path with an estimate of the fraction of shrub or forest along the flight path itself likely to affect the PBL (Figure 1, left). The forest/shrub cover along the flight path is estimated by averaging the percentage of forest/shrub cover per category over a length scale of 5 km, thus averaging over a few turbulent eddies with length scales comparable to the PBL depth [*Stull*, 1988]. Figure 1 thus highlights the variations in land surface types, dominated by shrubland, cropland, and forest, along the flight path. Of particular interest are the size of the heterogeneities, which range from kilometers to several tens of kilometers, as well as the apparent sharp boundaries between the shrub and cropland, which in the case of Parc W (protected), were known to be present.

[12] The impact of the land surface features identified with the GlobCover Land Cover product on the surface energy balance are assessed by using the land surface temperature produced by the Land Satellite Applications Facility (LandSAF) (available at http://landsaf.meteo.pt/) derived from observations made by the Meteosat Second Generation (MSG) satellite every 15 min. Additional cloud screening was applied to these data following *Taylor et al.* [2003]. Data between 0900 and 1000 UTC for 22 May to 10 October 2006 were averaged to produce the mean land surface temperature for the season. An estimate of the seasonal mean shallow cloud cover was also derived from MSG channel 1 visible (0.56–0.71 μm) data. This provides images every 15 min, which were logarithmically averaged (to reduce the impact of highly reflective events on the mean) along the flight path for June, July, and August of 2006 and 2007.

[13] The synoptic conditions on the day of the flight were quiet, with only weak northwesterlies across the Republic of Benin (Figure 2). As discussed in section 1, these light-wind conditions are expected to enhance the impact of any local or mesoscale effects. Furthermore, the 2 m air temperature trend shows no particular large-scale anomalies, with an approximately constant meridional temperature gradient in the northern region of the Republic of Benin. Channel 9 infrared (9.8–11.8 μm) data from the MSG satellite were used to look for any synoptic events that could affect conditions along the flight path. There was a decaying mesoscale convective system (MCS) moving from western Niger into eastern Mali, at approximately 18°N and 2°E during the aircraft measurements, but it had nearly completely dissipated by the time of the aircraft flight. A growing MCS was also moving westward from eastern Nigeria throughout the day (at approximately 10°N and 9°E during the aircraft measurements) but was too far away to exert any particular influence. Deep convection was also initiated a few kilometers west of the flight path during and after the aircraft runs. There was intermittent cloud presence along the flight trajectory, composed primarily of cumulus congestus, with some cumulonimbus and precipitation.

3. Mesoscale Circulation

[14] Figures 3 and 4 show aircraft data along the full track plotted as a function of latitude. Figures 3a and 3b show the liquid water and isoprene concentrations in the cloud run, and thus highlight the position of convective updrafts, given by the presence of cumulus congestus clouds. The presence of coincident peaks in the two demonstrates that for this case, in the absence of synoptically forced large-scale uplift, the presence in the cloud layer of chemical species emitted at the surface, such as isoprene, is exclusively brought about by small-scale convective updrafts, as practically every cloud measured has significant isoprene concentrations within. This leads to a distinctive isoprene distribution characterized by sharp spikes in the concentrations. In terms of the actual concentrations, the concentrations in the cloud layer can be very close to the PBL concentrations (Figure 4a), for example at 11.8°N, or considerably lower, such as at 11°N. It is likely that the cloud-level isoprene concentrations depend on both updraft strength and residence time

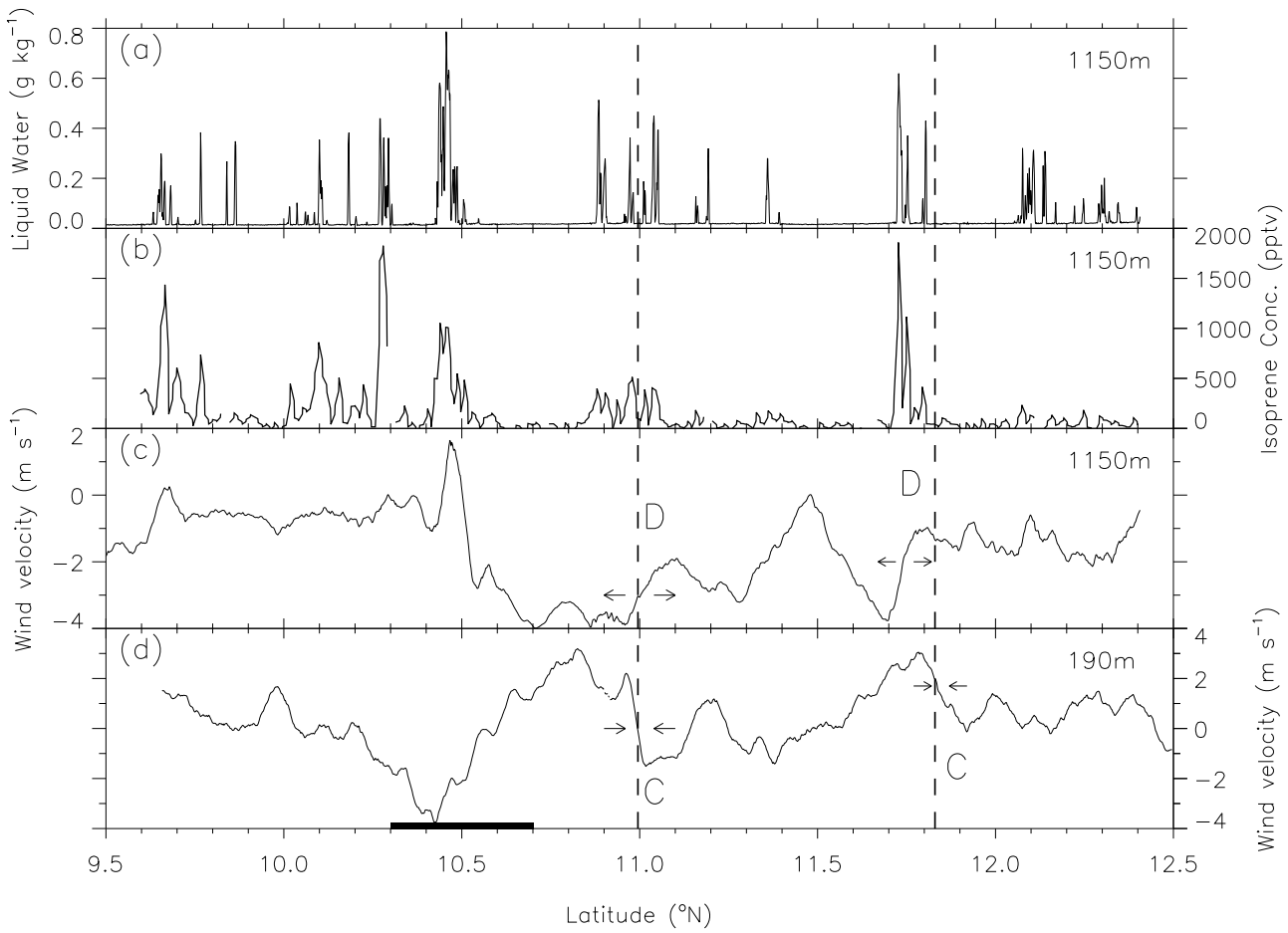

Figure 3. (a) Liquid water content from the Johnson Williams instrument, (b) isoprene concentration from the PTR-MS instrument, and (c and d) meridional component of wind velocity. The positions of two main areas of low-level convergence (C) are highlighted by the dashed lines, as well as the associated divergence zones (D) aloft. The black bar denotes the position of the convective downdraft. Figures 3a–3c are aircraft data taken along the cloud-level transect, and Figure 3d is aircraft data taken along the low-level transect.

(i.e., how much has decayed away) as well as the PBL concentrations below.

[15] From the aircraft data, the region 10.3°N–10.7°N along the flight path displays all the characteristics of a downdraft, namely, reduced PBL temperatures, reduced isoprene concentrations, and a peak in ozone concentrations (not shown), all consistent with the descent of high-altitude air. The cause of this downdraft can be attributed to the developing convection along the planned flight path, which was observed in the onboard radar and led to an eastward deviation from the north-south track between 9.6°N and 10.95°N. The PBL properties across this area will therefore not be closely related to the land surface, and this area is therefore not considered in this study.

[16] Figures 3c and 3d show the low-level and cloud-level meridional winds, which are closely aligned with the aircraft's trajectory. There is a negative relationship between the two on scales of tens of kilometers. The peaks in the low-level wind velocity at 10.8°N, 11.2°N, 11.8°N, 12°N, and 12.3°N all have an associated trough in the cloud-level wind velocity. This implies that the pattern is maintained throughout the two aircraft runs, which took just under 2 h to complete. The length and time scales exclude the possibility of turbulent eddies being the source of the observed organization of the winds. The observed relationship suggests on the other hand a persistent mesoscale forcing of the winds, which could be attributed either to the impact of the land surface, or a slow, mesoscale forcing such as a convergence line. Evidence is presented here that suggests that the former is the case. The areas of convergence and divergence produced by this mesoscale pattern of circulations also seem to coincide with cloud presence, particularly between 10.7°N and 12.0°N, which suggests a land surface organization of convection and, therefore, transport of chemical species into the cloud layer. Two particular low-level convergence zones are highlighted in Figure 3; these zones will be studied in more detail throughout this section. At 11°N one can observe the divergence in the meridional winds in the cloud layer directly above, with associated low, but significant, isoprene concentrations. At 11.8°N, however, there seems to be evidence of a sloping front, as the divergence aloft (and its associated liquid water and isoprene concentration peaks) are displaced southward by ~10 km with respect to the convergence zone 1 km below. There is a

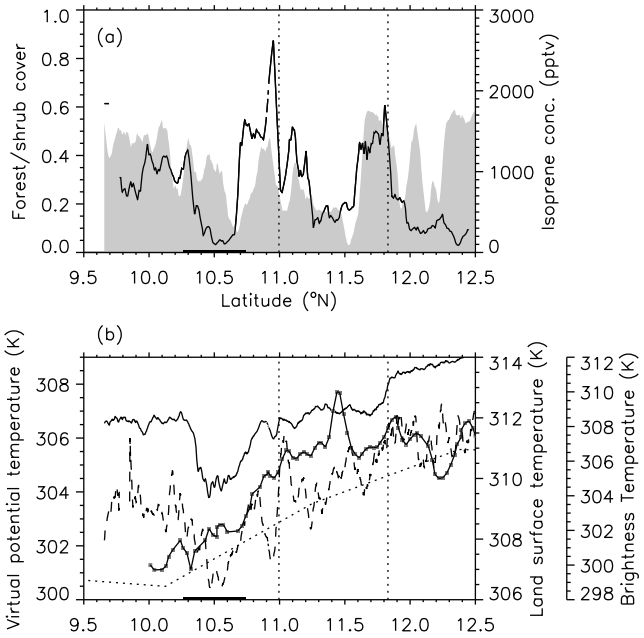

Figure 4. Data along the low-level flight path of (a) isoprene concentration from the PTR-MS instrument measured at 190 m on the low-level transect (solid line) and fraction of forest/shrub cover as derived from the GlobCover Land Cover map (shaded area) and (b) virtual potential temperature measured at 190 m on the low-level aircraft leg (solid), brightness temperature measured at 190 m on the low-level aircraft leg (dashed), virtual potential temperature at 956 hPa from the 1.125° resolution 1200 UTC ECMWF analysis (dotted), and land surface temperature from SEVIRI observations onboard the MSG satellite (squares). The vertical dotted lines show the positions of the two convergence zones identified in Figure 3, and the black bar denotes the position of the convective downdraft.

mean northerly flow in the cloud layer, and the ratio between the horizontal and vertical velocities in the lower level is 10, both of which are consistent with the presence of a sloping front, although some propagation between the two observation times is also possible.

[17] Figure 4 highlights the link between the convergence areas identified in Figure 3 and the land surface. Figure 4a broadly confirms the assumption that isoprene emissions are dominated by forest and shrub cover. The relationship is particularly strong between 10.7°N and 12.1°N, which is also the region where the mesoscale forcing of convection was most apparent. Furthermore, the large variations in isoprene, of over 1000 pptv, cannot be accounted for by variations in temperature or irradiance. This is particularly clear given that, as shown below, the peaks in isoprene concentrations coincide with negative temperature anomalies, which tend to decrease isoprene emissions [*Kesselmeier and Staudt*, 1999]. Although there is some ambiguity in the land surface classification, the strong isoprene concentrations over the shrubland suggest that the boundaries between the categories represent a distinct change in land surface properties. Similarly, considerable isoprene concentrations can be observed in the strip of shrubland running from 11°N, 2.5°E to 11.4°N, 2.8°E, and crossing the flight path at 11.2°N, although these shrubs are not a particularly prominent feature in Figure 1 (right). Two particular areas, however, show large deviations between the expected and observed isoprene concentrations. One is the previously identified downdraft region at 10.3°N–10.7°N, where the land surface and the PBL are not closely linked, because of the rapid injection of upper tropospheric air into the PBL through a downdraft. The other is in the northern region (>12.0°N), where there are particularly low isoprene concentrations over shrub and forestland. This is a feature which is present in all of the low-level flights with the BAe during the AMMA campaign over this region (not shown) and may be attributed either to the particular species that grow in this area or the vegetation densities being in the lower end of the land surface class range.

[18] The PBL and surface temperatures are closely linked to the land surface features (Figure 4b). The large-scale latitudinal increase in virtual potential temperature observed in the European Centre for Medium-Range Weather Forecasts (ECMWF) data is also observed in the virtual potential and brightness temperature trends as measured on the aircraft, as well as the seasonal-mean land surface temperature trend as derived from satellite data, although there seems to be a cool bias in the ECMWF analysis. At smaller scales it is clear that there are various negative anomalies in the land surface temperature of up to 2 K, a number of which are also observed in the PBL temperature and the brightness temperature. The brightness temperature is a good proxy for land surface temperature, so this suggests that the observed PBL temperature anomalies are strongly influenced by the land surface. Given that the land surface temperature is a seasonal mean, it implies that the temperature anomalies measured by the aircraft, particularly at the two main convergence zones highlighted by the dotted lines, are a climatological feature.

[19] Although no direct measurements of the PBL height were made, it is possible to estimate the impact of the observed temperature variations on the PBL height by using a single vertical potential temperature profile [*Carson*, 1973]. If one assumes that the potential temperature lapse rate above the PBL will remain constant throughout the day, it is possible to estimate the PBL height for a given increase in PBL potential temperature. The aircraft sampled a vertical profile along the flight track (11.9°N) between 1105 and 1120 UTC. Using this vertical potential temperature profile, it was estimated that the PBL height varied by 200 m K^{-1} along the flight path, with a PBL height of approximately 950 m for a PBL temperature of 303.5 K, as is observed for example between 11.3 and 11.8°N. The largest PBL temperature gradient, 2 K observed at 11.8°N, would therefore increase this value to 1350 m, whereas the PBL height within the cool temperature anomaly at 10.95°N would be approximately 750 m.

[20] There is a negative relationship between temperature anomalies and isoprene concentrations (Figures 4a and 4b) which is significant at the 95% level at wavelengths larger than 14 km (see section 4 for more details). The relationship also holds for the land surface temperature for latitudes below 12°N. At higher latitudes it is possible that seasonal variations in vegetation become more significant. Isoprene emissions, however, increase with increasing surface temperatures [*Kesselmeier and Staudt*, 1999]. One possible

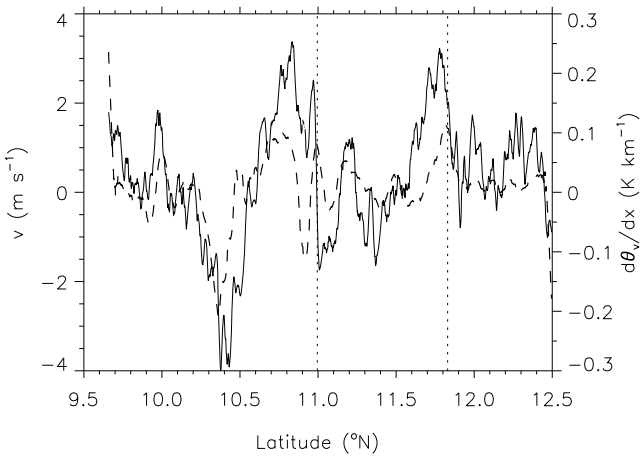

Figure 5. Aircraft data measured at 190 m along the low-level transect of meridional wind velocity (solid) and virtual potential temperature gradient (dashed). The vertical dotted lines show the positions of the two convergence zones identified in Figure 3.

explanation for this negative relationship is that the isoprene is mixed within a deeper boundary layer over the warmer surfaces, thus reducing (diluting) the concentrations. The PBL height estimates can be used to estimate the magnitude of this effect (as done, for example, by *Hopkins et al.* [2009]). The maximum observed temperature gradient is estimated to lead to an increase of 42% in the boundary layer depth associated with this increase in temperature. For equal emissions, this would lead to an approximate reduction in the isoprene concentrations of 30%. This alone cannot account for the drop in isoprene concentrations from 1800 to 700 pptv. Furthermore, there are larger isoprene gradients that are associated to much smaller temperature anomalies elsewhere along the domain, suggesting that the negative relationship between temperature (at the surface and in the PBL) and the isoprene concentrations must be due to the characteristics of the isoprene-emitting vegetation. It seems that higher evapotranspiration over the high isoprene-emitting shrubland, as opposed to the low isoprene-emitting cropland, leads to increased latent heat fluxes, an associated decrease in sensible heat fluxes, and thus to cool PBL temperature anomalies. These temperature anomalies also seem to persist throughout the season. It is proposed that the temperature gradients around these temperature anomalies then initiate land surface–induced flows, or vegetation breezes, which in turn organize the convection.

[21] The impact of these surface and atmospheric temperature gradients on the meridional winds is shown in Figure 5. First, the PBL temperature gradients, particularly in the convergence zones highlighted, are significant enough to induce mesoscale circulations, when compared to similar observational studies. *Taylor et al.* [2007], for example, observed mesoscale circulations forced by PBL gradients of $\sim$0.07–0.09 K km^{-1}, which are similar, if not smaller, than the gradients observed here. Although the temperature contrasts observed by *Taylor et al.* [2007] were of up to 3 K, as opposed to 2 K in this study, the sharp vegetation gradients associated with the boundaries of Parc W may lead to sharper temperature gradients. Second, there is a slightly lagged positive relationship between the meridional wind along the flight track and the gradient in PBL potential temperature, whose significance is computed in section 4 so that, in general, the peak in the PBL potential temperature gradient lies slightly north of the peak in wind velocity. More importantly, in practically all cases the peak in the temperature gradient coincides with a convergence zone. Thus, the convergence zones lie over the boundaries between the different vegetation types. For example, the divergence over the cool patch between 11.90°N and 12.05°N leads to convergence zones in the northern edge of the vegetative boundary (dotted line at 11.82°) and more weakly in the southern edge, at 12.05°N. This is also apparent at weaker convergence zones, such as at 10°N–10.2°N and 12.1°N. Furthermore, the relationship between temperature gradients and meridional winds throughout the domain suggest that these mesoscale flows are prevalent in the area.

4. Cospectral Analysis

[22] Cospectral analysis of the high-resolution aircraft data allows the quantification of length-scale dependences between variables. The spectral coherency can be regarded as a spectral equivalent to the correlation between two data sets. The cospectral analysis computes coherency as a function of length-scale, with a maximum value of 1 indicating perfect coherency, and 0 meaning the two data sets are not coherent with each other at that length-scale. The significance of correlations between atmospheric measurements is difficult to quantify because of the autocorrelation present within the data sets. This approach circumvents this problem, as the lowest length scales, where this autocorrelation occurs, can be ignored. Furthermore, it is possible to quantify the phase difference between data sets, highlighting the presence of any possible leads or lags between the variables. Using a spectral analysis outlined by *Matthews and Madden* [2000], and utilized in a similar fashion by *Taylor et al.* [2007], the spectral coherency was computed as a function of length scale. In order to eliminate the effect of the downdraft and because of the need of a continuous data set in the spatial scale, the cospectral analysis was only performed for data north of 10.7°N.

[23] Figure 6 shows a plot of the coherency squared as a function of wave number for the low-level potential temperature against the low-level meridional wind and isoprene concentrations, where wave number is defined as the reciprocal of the wavelength. There is a strong coherency between PBL potential temperatures and both wind speeds and isoprene concentrations. The relationship between potential temperature and wind speed is very significant down to wavelengths of 8 km (wave numbers less than 0.125). There is a second peak between 4 and 5 km, which could be either because of the effect of turbulent eddies [*Taylor et al.*, 2007] or boundary layer rolls (observed by *Marsham et al.* [2008] when comparing observations with large eddy model simulations). The coupling between PBL temperatures and isoprene concentrations remains significant down to 14 km, possibly extending down to 5 km. This is consistent with previous modeling and observational studies (e.g., *Baldi et al.* [2008] and *Taylor et al.* [2007], respectively) which show that at smaller length scales, below approximately 10 km, turbulent eddies will tend to disrupt any land surface impacts. The coherency between the low-level and cloud-

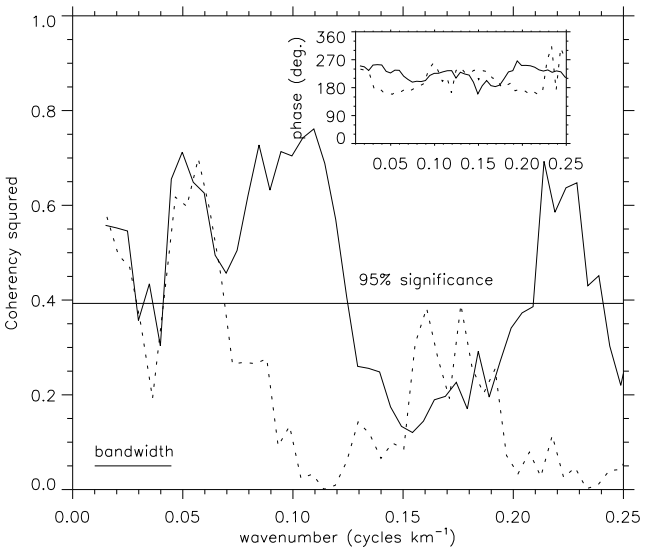

Figure 6. Coherency squared as a function of length scale for low-level virtual potential temperature and meridional wind velocity (solid) and virtual potential temperature and isoprene concentration (dotted). The inset shows the phase functions for these pairs of measurements as a function of length scale.

level meridional winds is over 95% significant for length scales between 30 and 50 km (not shown), consistent with what was observed in Figure 3.

[24] By estimating the eddy turnover time scales, it is possible to calculate the minimum length-scale of a land surface heterogeneity which can affect the whole boundary layer, L_{Rau}, for some atmospheric state. Given that the observed circulation affects the whole PBL, any coupling at length scales below L_{Rau} could not be associated to a land surface impact. This formulation, suggested by *Raupach and Finnigan* [1995], takes the form of

$$L_{\mathrm{Rau}} = C_{\mathrm{Rau}} \frac{U z_i}{w_*}, \tag{1}$$

where $C_{\mathrm{Rau}} = 0.8$ is an empirical nondimensional coefficient [*Mahrt*, 2000], U is the mean horizontal wind velocity, z_i is the PBL depth, and w_* is the Deardorff convective velocity scale. The aircraft data were used to estimate the PBL height, which was found to be approximately 1000 m, and the Deardorff convective velocity scale, which was estimated as 0.49 m s^{-1} [*Stull*, 1988]. U was estimated as 1.55 m s^{-1} by averaging the ECMWF wind speeds along the low-level flight path. These values give a minimum heterogeneity length scale of 2500 m, equivalent to a wavelength of 5000 m. L_{Rau} only represents a lower bound, so this estimate is consistent with the data.

[25] The inset in Figure 6 shows the phase difference, i.e., the leads/lags, between the variables. The phase between isoprene concentrations and PBL temperatures is of approximately 180° at all length-scales, particularly above 10 km, where the coupling is strongest. This confirms the negative relationship between the two that was observed in Figure 4. The phase relationship between wind speed and PBL temperatures, on the other hand, varies between 180° and 240°; this means that as one moves northward from cropland to an area with more woody vegetation, isoprene increases, temperature decreases (consistent with a decrease in Bowen ratio caused by higher evapotranspiration), and southerly winds increase (divergence). The convergence zones, however, do not occur directly over the vegetation boundaries, which would be associated with a phase of 180°, but are instead shifted toward the southern edge of the warm anomalies, as also observed in the work of *Taylor et al.* [2007]. As outlined in section 1, gravity currents moving against a weak synoptic wind will be shallower and more coherent than when moving in the same direction [*Goler and Reeder*, 2004; *Simpson and Britter*, 1980]. The ECMWF analysis shows a weak northwesterly synoptic flow (see Figure 2). Therefore, the northward moving component of the mesoscale flow is more coherent than the southward one, with enhanced convergence in the southern part of the warm anomalies, as observed. Figure 7 shows a schematic of the observed circulation illustrating these relationships. Finally, the synoptic flow moves toward the woody vegetation edge on the southern side of the warm anomalies. The increase in roughness length will lead to an increase in turbulence and drag and, thus, will also promote the convergence on the southern edge of the warm anomalies, as is observed for coastal convergence [e.g., *Malda et al.*, 2007].

[26] The gain as a function of length scale between the potential temperature and the wind velocity (not shown) represents the magnitude of the response of the wind to the PBL temperature variations. This was found to vary between 0.1 and 0.35 m s^{-1} K^{-1}, with a maximum at length scales of 20 km, consistent with *Wang et al.* [1996]. The lack of large variations in the gain confirms the robustness of the results, and these are also quantitatively comparable to the results found by *Taylor et al.* [2007].

5. Visible Satellite Data Climatology

[27] Vegetation heterogeneities vary only slowly in time, as compared for example to soil moisture anomalies, but do however have a very strong seasonal cycle. Early in the wet season (June) there will be stronger contrasts in leaf area and transpiration between crops and woody vegetation, as the latter will have access to deep soil water via well-established roots, while crops have not had time to develop to a great extent. Later in the season, however, the contrast will diminished as the crop's leaf area index develops rapidly. Overall, however, higher sensible heat fluxes are expected over the crop. Therefore, if cloud initiation is enhanced over the cropland, this should be a persistent feature throughout the season.

[28] A cloud climatology along the flight path was constructed from channel 1 data from the MSG satellite. In order to do this, the logarithmic mean of the channel 1 data was found for June, July, and August of 2006 and 2007. The logarithmic mean was used to reduce the impact of highly reflective events on the mean. In the absence of cloud, the channel 1 data give a measure of the reflectivity of the land surface, which depends both on the time of day and the albedo.

[29] In order to isolate the impact of clouds, for all data at time t after local noon, we subtracted the data at time t

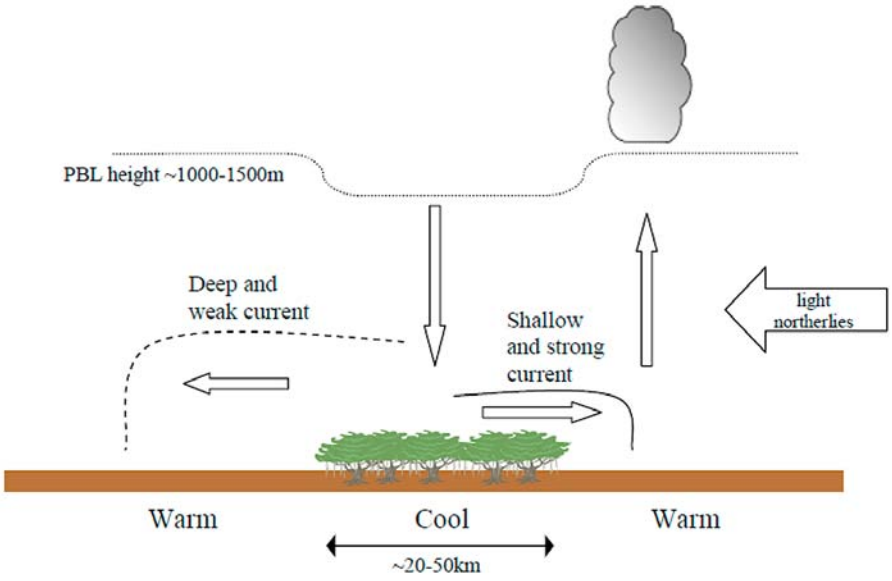

Figure 7. Schematic of the observed circulation as a result of vegetation heterogeneities. Over forested regions the PBL temperatures are cooler compared to the adjacent cropland, consistent with an increase in Bowen ratio caused by higher evapotranspiration. For heterogeneities on scales of ∼20–50 km, this leads to a circulation from the forest to the cropland. The presence of light northerly winds lead to a stronger northward flow as opposed to the southward flow, thus enhancing the updrafts and associated shallow cumulus and cumulus congestus clouds in the southern side of the warm anomalies.

before local noon. This then gave us the net impact of clouds, with a positive value denoting an enhancement of cloud in the afternoon and a negative value denoting an enhancement in the morning. Figure 8 shows the diurnal cycle of cloud cover along the flight path.

[30] First, we should note that in the absence of cloud the impact of both the time of day and the surface type could be expected to be symmetrical about local noon. This is not the case in practice since the measured reflectivity also depends on both the Sun and viewing angle. It is expected that this should lead, on average, to higher reflectivities in the morning as compared to the afternoon [*Roujean et al.*, 1992]. This would explain the predominance of negative values in Figure 8, particularly when comparing dusk and dawn, as well as the higher maximum for negative, as opposed to positive, values. Any positive anomaly in afternoon cloud will therefore be an underestimate and could be more significant than suggested by the plot.

[31] Figure 8 shows a bias toward more cloud in mid-afternoon (1.5–3.0 h), between 11.1°N and 11.8°N, with two peaks at 11.4°N and 11.55°N. This is consistent with the enhancement of cloud cover over the cropland, for example, when comparing to the region of reduced isoprene emissions between 11.2°N and 11.6°N. The match with the land surface temperature data, a more accurate reflection of the mean land surface impact throughout the season, is also consistent. The largest peak in the land surface temperature is between 11.35°N and 11.6°N, located in the center of the cropland, and the largest cloud cover lies just within the edges of this temperature anomaly. Earlier in the afternoon, at 1 h, there seem to be two smaller peaks at 11.2°N and 11.6°N, particularly noting that the background should be negative, rather than 0. This may be related to the initiation of clouds along the edges of the cropland boundaries. These clouds then develop into the more widespread signal observed later in the day (2–3 h), from 11.1°N–11.8°N. These results are consistent with previous statistical studies of satellite data, for example in the Amazon [*Cutrim et al.*, 1995; *Wang et al.*, 2009], and suggest that the circulations observed during the case study presented in this paper are not unique to this particular day and, in fact, could have a climatological impact on the presence of cloud in the region.

6. Discussion and Conclusions

[32] This study shows observations of a mesoscale organization of the winds persisting over 2 h, with areas of convergence which control patterns in the formation of cumulus congestus clouds. The organization is attributed to PBL temperature anomalies caused by variations in sensible heat flux at boundaries between forest/shrub and cropland. Isoprene is used as a tracer to link the surface characteristics, namely, woody cover, with meteorological variables, in order to ascertain the origin of the mesoscale organization and to illustrate the transport and mixing. Cospectral analysis is used to quantify the length scale dependence of these relationships, and it is shown that this vegetation-atmosphere interaction is significant down to wavelengths of 10 km, consistent with previous modeling and observational work. Finally, a visible satellite climatology along the flight track for the whole monsoon season suggests that these circulations have a climatological impact on the location of clouds in the early afternoon in the region.

[33] The aircraft observations also show that the convergence zones tend to occur on the southern edge of the warm anomalies. Convergence would be expected over the warm patches, as the flow would be maximized at the transition between vegetation types. However, the light northerly

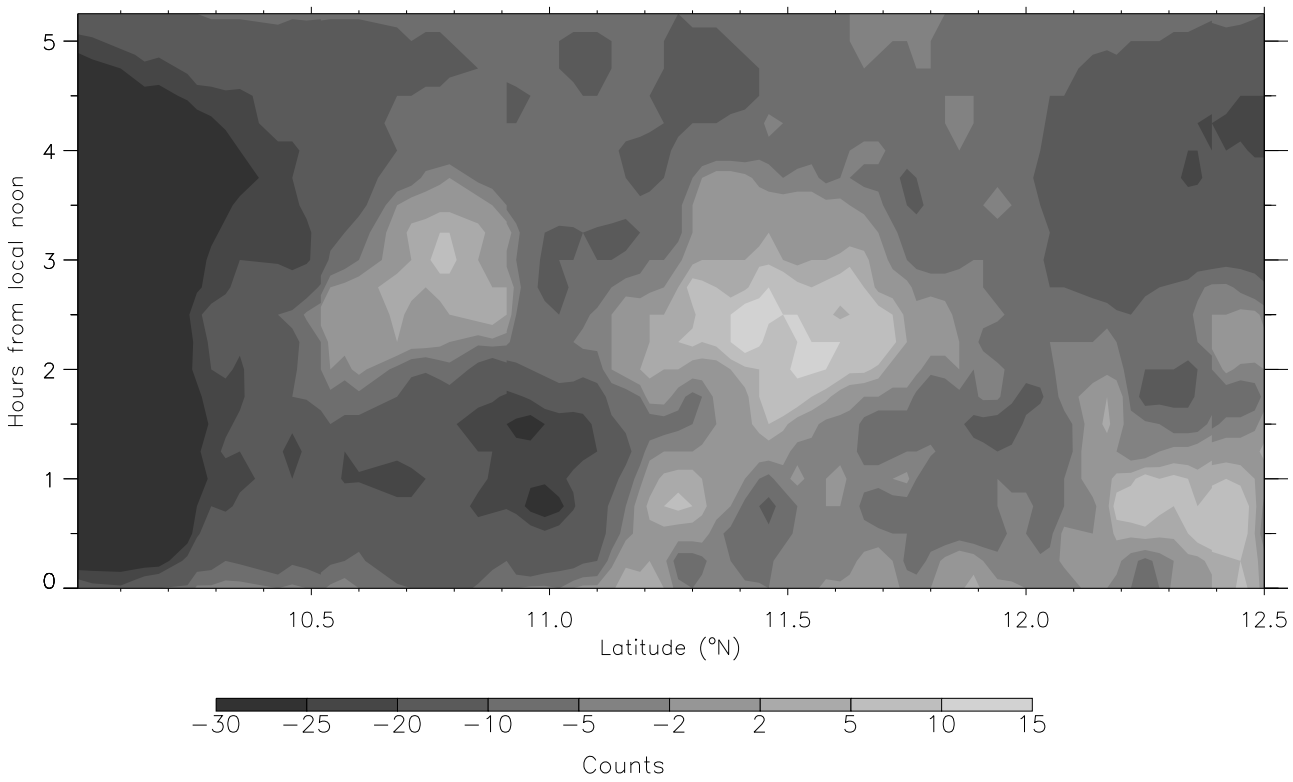

Figure 8. Hovmuller of Channel 1 data from the MSG satellite logarithmically averaged for June, July, and August of 2006 and 2007, with data from *t* minus local noon subtracted from *t* plus local noon. This gives an indication of cloud cover anomalies throughout the season in the afternoon (positive) and morning (negative).

synoptic wind, as observed in the 925 hPa ECMWF operational analysis, could be the cause of the southward displacement of the convergence zones, with stronger convergence on the southern sides of the warm anomalies, as well as an enhancement of turbulence, and hence the updrafts, associated with the flow toward the forest edge. Figure 7 shows a schematic of the observed circulation.

[34] There is considerable heterogeneity in land surface type in West Africa, brought about both by conversion of shrub and forestland into cropland, as well as the marked meridional transition from forest to semiarid land cover. Similar land surface features as observed on 17 August 2006 are found elsewhere in the region, particularly in the transition zone between forest and grassland south of approximately 12°N. The role of protected regions, as observed in the case study presented here, is also important, as the transition between protected and unprotected land can lead to the sharp vegetation gradients necessary to initiate mesoscale flows.

[35] Given the comparatively slow changes in vegetation cover, as opposed to soil moisture anomalies studied by *Taylor et al.* [2007], these features should be predictable in numerical weather prediction models. The correct prediction of shallow cumulus and cumulus congestus is particularly important for tropical convection. During the west African monsoon, the nocturnal jet transports humidity over the land by night in the lower levels, and this is then vertically distributed by day time convection [*Lothon et al.*, 2008; *Parker et al.*, 2005]. Using sounding data from the Tropical Ocean–Global Atmosphere Coupled Ocean–Atmosphere Response Experiment campaign in the western Pacific, *Parsons et al.* [2000] show how shallow moist convection and cumulus congestus, which occur even in the relatively adverse conditions present after the arrival of a dry intrusion, moisten the lower free troposphere, thus aiding in the recovery of conditions favorable to the occurrence of deep convection. Cumulus congestus clouds thus act as a precondition for the development of deep convection. Predicting areas of enhanced cumulus congestus cover could therefore be a prerequisite for the accurate forecast of larger-scale systems. Cumulus congestus are also significant for the correct prediction of the transport of chemical species emitted at the surface, such as isoprene, as they determine to what extent they are carried into the midtroposphere, and thus into the African Easterly Jet, which can then lead to long-range transport [*Sauvage et al.*, 2007].

[36] There are large variations between general circulation models in the prediction of future tropical convection. The Fourth Assessment Report (AR4) of the Intergovernmental Panel on Climate Change found that multimodel predictions of precipitation changes in 2080–2099 relative to 1980–1999 had an intermodel standard deviation exceeding the multimodel ensemble mean over most of the tropical regions, including West Africa, and less than 80% of the models agreed on the sign of the change [*Meehl et al.*, 2007]. Significant changes in land use and land cover are to be expected, be they deliberate or climate induced, as deforestation in West Africa already ranks as one of the highest in the world [*Myers*, 1991]. A better understanding of subgrid mesoscale land surface–atmosphere interactions

on the initiation of MCSs is therefore of significant importance to improve the prediction by global models of future precipitation in the region.

[37] More work is needed to ascertain the predominance and persistence of these flows in the region, particularly via the use of similar aircraft observations taken during the AMMA field campaign, as well as with the use of remote sensing products. The role of the diurnal and seasonal cycles observed in West Africa on these land surface effects needs to be assessed, particularly the evolution and impact of land surface–induced flows throughout the evening and into the night. Further evaluation of the land surface impact on mesoscale transport and mixing, for example, of chemical species such as isoprene, is also necessary, as these can lead to significant deviations from global model means (e.g., as observed by *Devine et al.* [2006] for cold pool outflows). The use of isoprene as a tracer for transport in this study is a first step in this direction. The ability of operational models to replicate these mesoscale phenomena also needs to be evaluated. To achieve these objectives, high-resolution modeling needs to be used in conjunction with the observations currently available for the region.

[38] **Acknowledgments.** On the basis of a French initiative, AMMA was built by an international scientific group and is currently funded by a large number of agencies, especially from France, the UK, the U.S. and Africa. This study was funded by the UK NERC project NE/B505538/1. LGC was funded by a NERC studentship NE/F007477/1. The authors would like to thank all those involved in the deployment of the FAAM aircraft. We would also like to acknowledge ESA and the ESA GlobCover Project, led by MEDIAS-France, for the use of the land surface data set, and the GLOBE Task Team and others for the use of the topography data set.

References

Andronache, C., W. L. Chameides, M. O. Rodgers, J. Martinez, P. Zimmerman, and J. Greenberg (1994), Vertical-distribution of isoprene in the lower boundary-layer of the rural and urban southern United-States, *J. Geophys. Res.*, *99*(D8), 16,989–16,999, doi:10.1029/94JD01027.

Atkinson, R. (1986), Kinetics and mechanisms of the gas-phase reactions of the hydroxyl radical with organic-compounds under atmospheric conditions, *Chem. Rev.*, *86*(1), 69–201, doi:10.1021/cr00071a004.

Avissar, R., and T. Schmidt (1998), An evaluation of the scale at which ground-surface heat flux patchiness affects the convective boundary layer using large-eddy simulations, *J. Atmos. Sci.*, *55*(16), 2666–2689, doi:10.1175/1520-0469(1998)055<2666:AEOTSA>2.0.CO;2.

Baldi, M., et al. (2008), Vertical velocities and available potential energy generated by landscape variability—Theory, *J. Appl. Meteorol. Climatol.*, *47*(2), 397–410, doi:10.1175/2007JAMC1539.1.

Brown, M. E., and D. L. Arnold (1998), Land-surface-atmosphere interactions associated with deep convection in Illinois, *Int. J. Climatol.*, *18*(15), 1637–1653, doi:10.1002/(SICI)1097-0088(199812)18:15<1637::AID-JOC336>3.0.CO;2-U.

Carson, D. J. (1973), Development of a dry inversion-capped convectively unstable boundary-layer, *Q. J. R. Meteorol. Soc.*, *99*(421), 450–467, doi:10.1002/qj.49709942105.

Cutrim, E., et al. (1995), Enhancement of cumulus clouds over deforested lands in Amazonia, *Bull. Am. Meteorol. Soc.*, *76*(10), 1801–1805, doi:10.1175/1520-0477(1995)076<1801:EOCCOD>2.0.CO;2.

Devine, G. M., K. S. Carslaw, D. J. Parker, and J. C. Petch (2006), The influence of subgrid surface-layer variability on vertical transport of a chemical species in a convective environment, *Geophys. Res. Lett.*, *33*, L15807, doi:10.1029/2006GL025986.

Doran, J. C., et al. (1995), Boundary-layer characteristics over areas of inhomogeneous surface fluxes, *J. Appl. Meteorol.*, *34*(2), 559–571.

Fisch, G., et al. (2004), The convective boundary layer over pasture and forest in Amazonia, *Theor. Appl. Climatol.*, *78*(1–3), 47–59, doi:10.1007/s00704-004-0043-x.

Goler, R. A., and M. J. Reeder (2004), The generation of the morning glory, *J. Atmos. Sci.*, *61*(12), 1360–1376, doi:10.1175/1520-0469(2004)061<1360:TGOTMG>2.0.CO;2.

Guenther, A., et al. (1995), A global-model of natural volatile organic-compound emissions, *J. Geophys. Res.*, *100*(D5), 8873–8892.

Hong, X. D., et al. (1995), A sensitivity study of convective cloud formation by vegetation forcing with different atmospheric conditions, *J. Appl. Meteorol.*, *34*(9), 2008–2028, doi:10.1175/1520-0450(1995)034<2008:ASSOCC>2.0.CO;2.

Hopkins, J. R., et al. (2009), Direct estimates of emissions from the megacity of Lagos, *Atmos. Chem. Phys.*, *9*(21), 8471–8477.

Kang, S. L., et al. (2007), Observations of the ABL structures over a heterogeneous land surface during IHOP_2002, *J. Hydrometeorol.*, *8*(2), 221–244, doi:10.1175/JHM567.1.

Kesselmeier, J., and M. Staudt (1999), Biogenic volatile organic compounds (VOC): An overview on emission, physiology and ecology, *J. Atmos. Chem.*, *33*(1), 23–88, doi:10.1023/A:1006127516791.

Lebel, T., et al. (2009), AMMA-CATCH studies in the Sahelian region of West-Africa: An overview, *J. Hydrol.*, *375*, 3–13, doi:10.1016/j.jhydrol.2009.03.020.

Linden, P. F., and J. E. Simpson (1986), Gravity-driven flows in a turbulent fluid, *J. Fluid Mech.*, *172*, 481–497, doi:10.1017/S0022112086001829.

Liss, P. S., and L. Merlivat (1986), Air-sea gas exchange rates: Introduction and synthesis, in *The Role of Air-Sea Interactions in Geochemical Cycling*, edited by P. Buat-Menard, pp. 113–129, Springer, New York.

Lothon, M., et al. (2008), Observation of the diurnal cycle in the low troposphere of West Africa, *Mon. Weather Rev.*, *136*(9), 3477–3500, doi:10.1175/2008MWR2427.1.

Mahrt, L. (2000), Surface heterogeneity and vertical structure of the boundary layer, *Boundary Layer Meteorol.*, *96*(1–2), 33–62, doi:10.1023/A:1002482332477.

Malda, D., et al. (2007), The role of atmospheric boundary layer-surface interactions on the development of coastal fronts, *Ann. Geophys.*, *25*(2), 341–360.

Marsham, J. H., et al. (2008), Observations of mesoscale and boundary-layer scale circulations affecting dust transport and uplift over the Sahara, *Atmos. Chem. Phys.*, *8*(23), 6979–6993.

Matthews, A. J., and R. A. Madden (2000), Observed propagation and structure of the 33-h atmospheric Kelvin wave, *J. Atmos. Sci.*, *57*(21), 3488–3497, doi:10.1175/1520-0469(2000)057<3488:OPASOT>2.0.CO;2.

Meehl, G. A., et al. (2007), Global Climate Projections, in *Climate Change 2007: The Physical Science Basis. Contribution of Working Group I to the Fourth Assessment Report of the Intergovernmental Panel on Climate Change*, edited by S. Solomon et al., pp. 589–662, Cambridge Univ. Press, Cambridge, New York.

Myers, N. (1991), Tropical forests: Present status and future outlook, *Clim. Change*, *19*(1–2), 3–32, doi:10.1007/BF00142209.

Parker, D. J. (1998), The dependence of cold-pool depth on source conditions, *Mon. Weather Rev.*, *126*(2), 516–520, doi:10.1175/1520-0493(1998)126<0516:TDOCPD>2.0.CO;2.

Parker, D. J., et al. (2005), The diurnal cycle of the West African monsoon circulation, *Q. J. R. Meteorol. Soc.*, *131*(611), 2839–2860, doi:10.1256/qj.04.52.

Parsons, D. B., et al. (2000), The evolution of the tropical western Pacific atmosphere-ocean system following the arrival of a dry intrusion, *Q. J. R. Meteorol. Soc.*, *126*(563), 517–548, doi:10.1002/qj.49712656307.

Pielke, R. A., Sr. (2001), Influence of the spatial distribution of vegetation and soils on the prediction of cumulus convective rainfall, *Rev. Geophys.*, *39*(2), 151–177, doi:10.1029/1999RG000072.

Pinty, J.-P., et al. (1989), An investigation of mesoscale flows induced by vegetation inhomogeneities using an evapotranspiration model calibrated against HAPEX-MOBILHY data, *J. Appl. Meteorol.*, *28*(9), 976–992, doi:10.1175/1520-0450(1989)028<0976:AIOMFI>2.0.CO;2.

Rabin, R. M., et al. (1990), Observed effects of landscape variability on convective clouds, *Bull. Am. Meteorol. Soc.*, *71*(3), 272–280, doi:10.1175/1520-0477(1990)071<0272:OEOLVO>2.0.CO;2.

Raupach, M. R., and J. J. Finnigan (1995), Scale issues in boundary-layer meteorology - surface-energy balances in heterogeneous terrain, *Hydrol. Process.*, *9*(5–6), 589–612, doi:10.1002/hyp.3360090509.

Redelsperger, J. L., et al. (2006), African monsoon multidisciplinary analysis: An international research project and field campaign, *Bull. Am. Meteorol. Soc.*, *87*(12), 1739–1746, doi:10.1175/BAMS-87-12-1739.

Roujean, J. L., M. Leroy, and P.-Y. Deschamps (1992), A bidirectional reflectance model of the Earth's surface for the correction of remote-sensing data, *J. Geophys. Res.*, *97*(D18), 20,455–20,468.

Sauvage, B., et al. (2007), Medium-range mid-tropospheric transport of ozone and precursors over Africa: Two numerical case studies in dry and wet seasons, *Atmos. Chem. Phys.*, *7*(20), 5357–5370.

Segal, M., and R. W. Arritt (1992), Nonclassical mesoscale circulations caused by surface sensible heat-flux gradients, *Bull. Am. Meteorol. Soc.*, *73*(10), 1593–1604, doi:10.1175/1520-0477(1992)073<1593:NMCCBS>2.0.CO;2.

Segal, M., et al. (1995), Scaling evaluation of the effect of surface characteristics on potential for deep convection over uniform terrain, *Mon.*

Weather Rev., *123*(2), 383–400, doi:10.1175/1520-0493(1995)123<0383:SEOTEO>2.0.CO;2.

Simpson, J. E., and R. E. Britter (1980), A laboratory model of an atmospheric mesofront, *Q. J. R. Meteorol. Soc.*, *106*(449), 485–500, doi:10.1002/qj.49710644907.

Smith, E. A., et al. (1994), Linking boundary-layer circulations and surface processes during Fife-89. 1. Observational analysis, *J. Atmos. Sci.*, *51*(11), 1497–1529, doi:10.1175/1520-0469(1994)051<1497:LBLCAS>2.0.CO;2.

Souza, E. P., et al. (2000), Convective circulations induced by surface heterogeneities, *J. Atmos. Sci.*, *57*(17), 2915–2922, doi:10.1175/1520-0469(2000)057<2915:CCIBSH>2.0.CO;2.

Strapp, J. W., and R. S. Schemenauer (1982), Calibrations of Johnson-Williams liquid water-content meters in a high-speed icing tunnel, *J. Appl. Meteorol.*, *21*(1), 98–108, doi:10.1175/1520-0450(1982)021<0098:COJWLW>2.0.CO;2.

Stull, R. B. (1988), *An Introduction to Boundary Layer Meteorology*, 666 pp., Kluwer Acad., London.

Taylor, C. M., et al. (2003), Linking boundary-layer variability with convection: A case-study from JET2000, *Q. J. R. Meteorol. Soc.*, *129*(592), 2233–2253, doi:10.1256/qj.02.134.

Taylor, C. M., D. J. Parker, and P. P. Harris (2007), An observational case study of mesoscale atmospheric circulations induced by soil moisture, *Geophys. Res. Lett.*, *34*, L15801, doi:10.1029/2007GL030572.

Taylor, C. M., et al. (2009), Impact of soil moisture on the development of a Sahelian mesoscale convective system: A case-study from the AMMA special observing period, *Q. J. R. Meteorol. Soc.*, doi:10.1002/qj.465, in press.

Trier, S. B., et al. (2004), A study of convection initiation in a mesoscale model using high-resolution land surface initial conditions, *Mon. Weather Rev.*, *132*(12), 2954–2976, doi:10.1175/MWR2839.1.

Wang, J. F., et al. (1996), A stochastic linear theory of mesoscale circulation induced by the thermal heterogeneity of the land surface, *J. Atmos. Sci.*, *53*(22), 3349–3366, doi:10.1175/1520-0469(1996)053<3349:ASLTOM>2.0.CO;2.

Wang, J. F., et al. (2009), Impact of deforestation in the Amazon basin on cloud climatology, *Proc. Natl. Acad. Sci. U. S. A.*, *106*(10), 3670–3674, doi:10.1073/pnas.0810156106.

Weaver, C. P. (2004), Coupling between large-scale atmospheric processes and mesoscale land-atmosphere interactions in the U.S. Southern Great Plains during summer. Part I: Case studies, *J. Hydrometeorol.*, *5*(6), 1223–1246, doi:10.1175/JHM-396.1.

Wilson, J. W., and W. E. Schreiber (1986), Initiation of convective storms at radar-observed boundary-layer convergence lines, *Mon. Weather Rev.*, *114*(12), 2516–2536, doi:10.1175/1520-0493(1986)114<2516:IOCSAR>2.0.CO;2.

L. Garcia-Carreras and D. J. Parker, Institute for Climate and Atmospheric Science, University of Leeds, Leeds LS2 9JT, UK. (eelgc@leeds.ac.uk)

J. G. Murphy, Department of Chemistry, University of Toronto, 80 Saint George St. Toronto, ON M5S 3H6, Canada.

C. E. Reeves, School of Environmental Science, University of East Anglia, Norwich NR4 7TJ, U.K.

C. M. Taylor, Centre for Ecology and Hydrology, Wallingford OX10 8BB, UK.